IOP Publishing Superconductor Science and Technology
Supercond. Sci. Technol. 31 (2018) 095004 (10pp) https://doi.org/10.1088/1361-6668/aad278

An equivalent homogenized model for non-superconducting joints made by ReBCO coated conductors

Yunhao Pan, Wei Wu, Jie Sheng, Xiaofen Li, Fangliang Dong, Mingyang Wang, Yue Zhao, Zhiwei Zhang, Zhuyong Li, Zhen Huang, Zhiyong Hong and Zhijian Jin

Department of Electrical Engineering, Shanghai Jiao Tong University, No. 800 Dongchuan Road, Minhang District, Shanghai, 200240, People's Republic of China

E-mail: wei.wu@sjtu.edu.cn

Received 24 December 2017, revised 19 June 2018
Accepted for publication 10 July 2018
Published 30 July 2018

Abstract

The most popular method of reducing joint resistance R_j is by increasing overlap length l. A numerical model capable of simulating the relationship between joint resistance and overlap length (the log(R_j)–log(l) curve) could provide guidance for commercial high temperature superconducting joint manufacturing and may shed light on some more detailed behavior. In this study, a three-dimensional model with an equivalent single homogeneous layer, characterized by resistance per unit area ρ_s ($\Omega\,m^2$), is developed and tested against experimental data. With this model, detailed measurement of parameters such as the thickness and resistivity of each layer and the interfacial resistance are not necessary. The log(R_j)–log(l) relationship, especially for longer joints ($l > 20$ cm), can be predicted by employing only ρ_s, which can be experimentally and accurately obtained from shorter joints ($l \leqslant 20$ cm). The log(R_j)–log(l) curve exhibits a nonlinear relationship when the overlap length exceeds a certain threshold value, in contrast to the commonly considered $R_j = \rho_s/wl$ relationship (where w is the width of the joining area). This result is validated by accurately measuring the resistance of soldered joints with overlap lengths of 5–90 cm. The sensitivity of simulation results by different n values, I_j/I_c, and meshing precision levels are also presented.

Keywords: HTS, homogenization techniques, coated conductor, field decay method, resistive joints, soldered joints, finite element analysis

(Some figures may appear in colour only in the online journal)

1. Introduction

Second-generation (2G) high temperature superconducting (HTS) coated conductors (CCs) are promising for various large superconducting magnets, such as those for MRI/NMR and maglev applications, because of their higher critical current density at high magnetic fields and lower cooling costs [1, 2]. All these magnets need suitable joints to form closed-loop circuits and hence operate in persistent current mode [3, 4]. The joint resistance R_j should be minimized because these magnets require an extremely low magnetic field decay rate. For MRI and NMR, the magnetic field decay rate must be at most 0.05 ppm h^{-1}, and hence joint resistance at pico-ohm level is required [5, 6]. Even for cases such as maglev, in which the decay rate limit is 1%/day [7–10], and joint resistance at the nano-ohm level is a basic requirement. Superconducting joints of 2G-HTS tapes have been achieved in recent years [11–14]. However, because practical superconducting joints between CCs are currently difficult to obtain, one may ask if joint resistance at the pico-ohm level can be achieved by simply increasing the joining length, according to

$$R_j = \frac{\rho_s}{w \cdot l}, \tag{1}$$

where ρ_s is the layer equivalent resistance per unit area. Therefore, it is important to build a simulation model that can

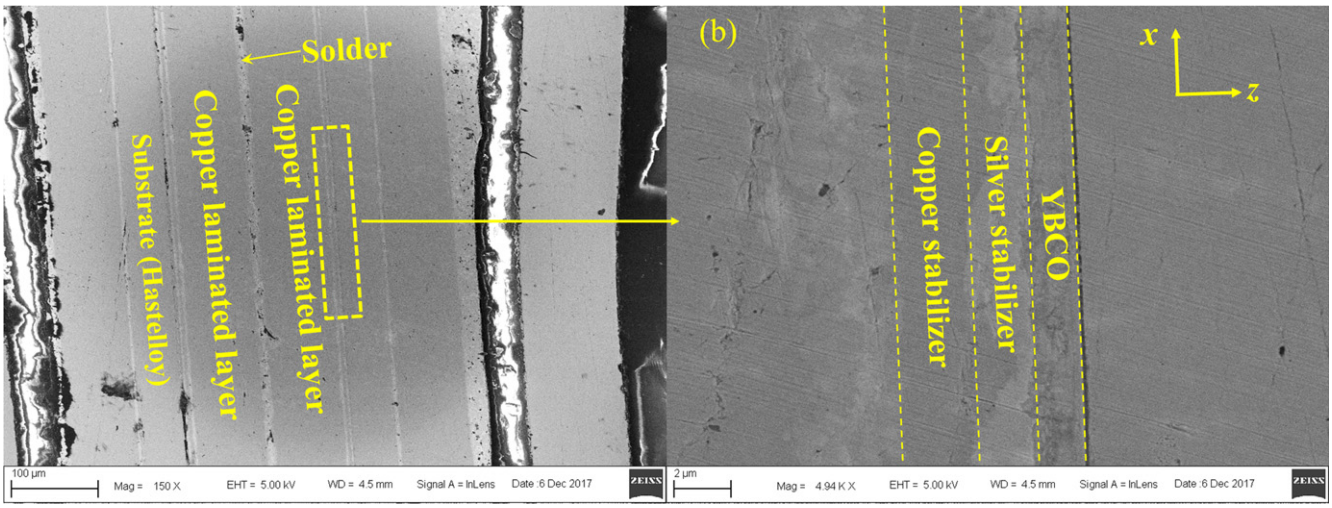

Figure 1. (a) SEM images of a soldered joint with $Pb_{38}Sn_{62}$ solder (YBCO tapes are laminated by copper stripes); (b) enlarged view of the corresponding position (mainly showing the YBCO layer, silver stabilizer layer, and copper stabilizer layer).

predict the relationship between R_j and l (the R_j–l curve) and current distribution [15].

However, there are two main difficulties in building and verifying a joint simulation model: first, the structure of the connection layers between two ReBCO layers is complicated [16], as shown in figure 1. The joint material in between the two YBCO layers is composed of many sublayers with different material properties [17]. Interfacial resistance between these layers is also present. Furthermore, the thickness of each sublayer is not uniform; therefore, this multilayer structure geometry is difficult to reconstruct in the simulation model. Second, the precise measurement of some parameters such as the thickness and resistivity of the interfacial resistance is unavailable.

In the intermediate resistive layers, the current density is by far orthogonal to the joint contact plane, which implies that the equipotential surfaces are locally quasi-parallel to the joint plane and that it is possible to define the layer equivalent resistance per unit area ρ_s ($\Omega\,m^2$), which is a measurable parameter according to the direct measurement of R_j, l, and w.

In this paper, a simplified structure model is established, which considers only one single-equivalent homogeneous layer to connect two YBCO layers. The equivalence between the simplified structure model and multilayer structure model is demonstrated by comparing their J_z (x, y) distributions. On the basis of this model, we observed that the equivalent resistance per unit area ρ_s, which can be precisely determined, is the dominant factor for the log(R_j)–log(l) curve tendency and J_z (x, y) distribution. A series of soldered joints with different overlap lengths (3–90 cm) are fabricated and measured for verifying this model. ρ_s is determined from the shorter joints (3–20 cm) and it is then used to successfully predict the behavior of the longer joints (40–90 cm) from the model. The tendency of the log(R_j)–log(l) curve shows a nonlinear saturated phenomenon when the overlap length exceeds a certain threshold value. The joint resistance tends to a finite limit value instead of continuously declining according to equation (1). The sensitivity of simulation results by different n values, I_j/I_c, and meshing precision are presented.

2. Simulation model and experimental data processing

2.1. Fundamental theory

The basic equations used in this model are Faraday's law and Ampère's law. In this three-dimensional (3D) problem, the components of the magnetic field strength H_x, H_y, and H_z are the state variables [18–23]. The physical characteristics of a superconductor material are modeled by a nonlinear E–J power law.

The connection layer between two YBCO layers consists of many sublayers (such as stabilizer layers and protection layers), interfacial resistance, and joining materials [24]. The mathematical conversion process from a multilayer structure to a single layer structure is described here.

According to Joule's law, the joint resistance R_j can be calculated by

$$I_j^2 \cdot R_j = \int \mathbf{E} \cdot \mathbf{J} dxdydz. \tag{2}$$

For the 3D current distribution in the connection layer, as a general result, J_z is by far the dominant component of the current density [25, 26]. Joule loss induced by J_z is the dominant component of the total loss, which are four and six orders of magnitude higher than the loss induced by J_x and J_y, respectively. Hence, R_j can be given by

$$\begin{aligned} R_j &\approx \frac{1}{I_j^2} \iiint (E_z \cdot J_z) dxdydz \\ &= \frac{1}{I_j^2} \iiint \rho(z) \cdot J_z{}^2(x, y, z) dxdydz. \end{aligned} \tag{3}$$

Because J_z is almost uniform along the thickness direction (z-direction) in the multilayer structure, the x–y surface integral of $J^2(x, y)$ is considered to be a constant in the z-direction. R_j can be written as

$$R_j = \frac{1}{I_j^2} \cdot \int \rho(z) dz \iint J_z{}^2(x, y) dxdy. \tag{4}$$

Therefore, the line integral of bulk resistivity over the z-direction for each sublayer in the connection layer may be

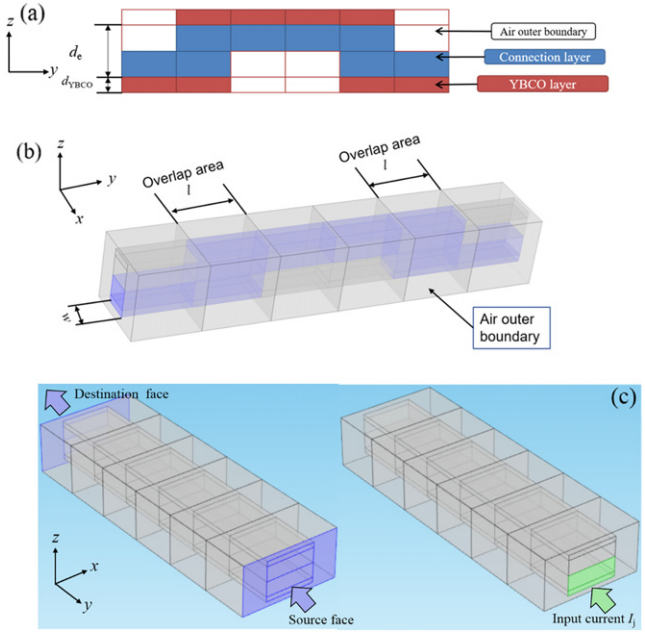

Figure 2. Geometry sketch map of the simulation model. (a) The z–y plane view of the joint model, (b) 3D view of the joint model (the purple area is the joint geometry and the gray area is the air area), and (c) the area where the boundary conditions are applied in the simulation model. The joint domains are magnified in the sketch map. In the simulation model, the air domains are much bigger than joint domains.

converted into a single layer form:

$$\rho_s = \int \rho(z) dz. \tag{5}$$

This is a constant value for a certain joint structure and can be precisely measured by experiments for cases in which $R_j = \rho d/lw$ holds without consideration of the resistivity and thickness of each sublayer.

2.2. Model establishment

All the simulation models are implemented in the partial differential equation module of the finite element software package COMSOL Multiphysics 5.1. A typical joint model geometry is shown in figure 2, the x, y and z directions correspond to the width, length and thickness direction, respectively. The connection layer between two YBCO layers is considered as one single-equivalent homogeneous layer, which is illustrated in figure 3. d_{YBCO} is the thickness of the YBCO layer and d_e is the thickness of the single-equivalent homogeneous layer. This model uses the swept mesh method, and the source face and the destination face are marked with purple as shown in figure 2(c). The source face is meshed by free triangular elements with the 'finer' element size, which is a predefined size in COMSOL. The periodic boundary condition is employed and applied to the source and destination faces to make the solution equal on two selected boundaries. The current I_j is input in the green boundary as shown in figure 2(c) by a constraint boundary condition.

2.3. Experimental method

The soldered joints are made from YBCO tapes manufactured by Shanghai Superconductor Technology Co., Ltd. YBCO tapes are coated with copper; their parameters are summarized in table 1. The jointing material is Sn63Pb37 solder [27, 28], with a resistivity of $1.45 \times 10^{-7}\,\Omega\,\mathrm{m}$. The structure of the experimental joint is a lap (shake hand) joint and bridge joint (which is the concatenation of two lap joints). The tapes are stacked together with the YBCO sides face-to-face. In this joint structure, the copper stabilizer layers of two tapes are in contact. A non-corrosive solder flux is applied prior to soldering. The YBCO tapes are heated to 300 °C in a well-controlled manner. Further, the tapes are gently contacted with the soldering iron until the solder flowed on the surface of the tapes. After the assembly, the excess solder or flux residue in the soldered joint is removed.

2.4. Joint resistance measurement and data processing

Generally speaking, the joint resistance is calculated as the slope of the voltage versus current characteristic curve (V–I curve) for a transport current that is lower than the critical current [29, 30]. The typical behavior of the voltage–current characteristic of a joint in DC can be described by this equation

$$V = R_j \cdot I + l \cdot V_c \cdot \left(\frac{I}{I_c}\right)^{n_j}, \tag{6}$$

where V_c is the criterion voltage of $1\ \mu\mathrm{V\,cm^{-1}}$ and I_c is the current when the voltage is V_c (at 77 K), n_j is the n value of joint, notice that n_j can be different from the conductor n value. The shorter (l = 3–20 cm) lap joints are measured by the V–I method. In actual measurements, when the resistance of the longer joint is less than 1 nΩ, the fluctuation of data points in the V–I curve becomes wildly scattered. This is likely due to measurement system errors. Because the V–I curve method uses all the data points before I_c indiscriminately, the system error may become larger when the joint resistance is lower and is difficult to describe quantitatively.

In order to solve this problem, longer joints are measured by the field decay method. The field decay method measures joint resistance from the temporal decay of the current or magnetic field of a closed-loop coil, and has high measurement precision [1]. Currents are induced in the closed-loop coil by the persistent current switch controlled by heat [31, 32]. The closed-loop coil can be equivalent to a standard L–R circuit, and therefore the decay of its magnetic field B follows

$$B = B_0 \cdot e^{-\frac{R_j}{L}t}, \tag{7}$$

$$\ln(B) = \ln(B_0) - \frac{R_j}{L}t, \tag{8}$$

where L is the inductance value of the measured coil and determined by simulation in this work. The joint for closed-loop coil is bridge structure that is composed by two lap joints in series consecutively. The $\ln(B) - t$ curve for closed coils

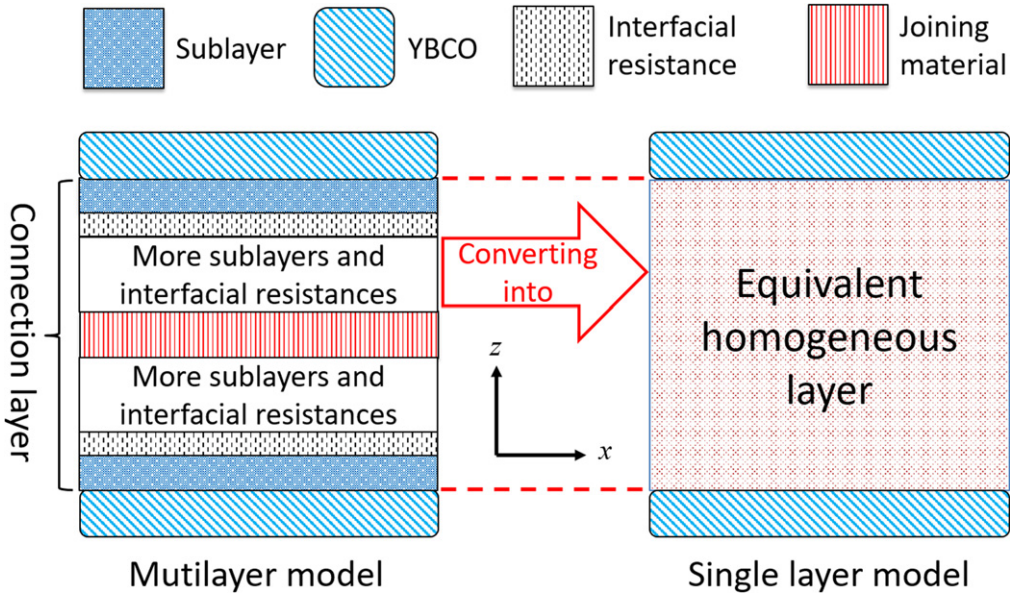

Figure 3. Equivalent relationship schematic between the single layer model and multilayer model.

Table 1. Detailed parameters of YBCO tapes (as the global parameters in simulation models).

Parameter		Value
Thickness (mm)	Total tape	0.06
	YBCO layer	0.001
	Cu stabilizer layer	0.01
	Ag protection layer	0.003
	Substrate	0.045
Critical current (A)		250
n (n_x, n_y, n_z)		39
w (mm)		10
E_{cx}, E_{cy}, E_{cz}(V m^{-1})		1.0×10^{-4}
J_{cx}, J_{cy}(A m^{-2})		2.5×10^{10}
J_{cz}(A m^2)		2.5×10^{7}
μ_r		1
μ_0 (H m^{-1})		$4\pi \times 10^{-7}$

with 50 and 90 cm joints are shown in figure 4 as examples. It exhibits a perfect linearity between ln(B) and t, which corresponds to the high accuracy of our measurement.

3. Current density distribution in the multilayer and single layer models and significance of ρ_s

3.1. The current density distribution in the multilayer model and single layer model

In this section, a theoretical comparison of current distribution between the multilayer and single layer model is presented to verify their equivalence. According to the analysis in section 2.2, the J_z distribution in the single layer model and multilayer structure model should be as similar as possible if these two models are equivalent. Therefore, the J_z distributions (cross section is located at the middle of each layer in the z-axis) in the equivalent homogeneous layer of the simplified model and different sublayers of the multilayer structure model are simulated as an example, as illustrated in figure 5. Under the same parameters ($l = 5$ cm, $d_{YBCO} = 0.01$ mm, $w = 10$ mm, $I_j = 100$ A), we set four equal-thickness sublayers, (b1)–(b4) in the multilayer structure model (the interfacial resistance is not set in the multilayer model because its essence is an extremely thin sublayer in the connection layer [33, 34]); layer (a) refers to the equivalent homogeneous layer. The detailed parameters in these two models according to equation (5) are shown in table 2; the values of $\rho_{b1} \sim \rho_{b4}$ and $d_{b1} \sim d_{b4}$ are assumed values that do not represent any real materials. The J_z distribution in layer (a) and layers (b1)–(b4) are nearly the same, which means $\iint J_z^2(x, y, z)dxdy$ in these two models are nearly identical. According to section 2.2, R_j will remain the same after model simplification.

3.2. Significance of ρ_s

When equation (4) holds, the same results can be obtained for different combinations of ρ_e and d_e. In this way, in the f.e.m. mesh, the thickness of very thin layers may be artificially increased to improve the mesh quality in terms of thickness-length ratio.

In general, finite element software such as COMSOL has little ability to solve geometries with low thickness-length ratios. Figure 6 plots the J_z distributions under different combinations of ρ_e and d_e with ρ_s set to a constant value, where the values of l, d_{YBCO}, w, and I_j are the same as those in section 3.1. Table 3 lists the detailed values of ρ_s used in this section. The J_z distributions in the equivalent layers (e1)–(e4) are nearly equal to each other. The change in ρ_e and d_e would not change the validity of the single layer model when ρ_s is set to a constant value.

The J_z distributions in figure 6 indicate that the x–y surface integrals of J_z^2 (x, y, z) in equation (4) are also approximately the same under different combinations of ρ_e and d_e (keeping ρ_s constant). Therefore, according to section 2.1, the

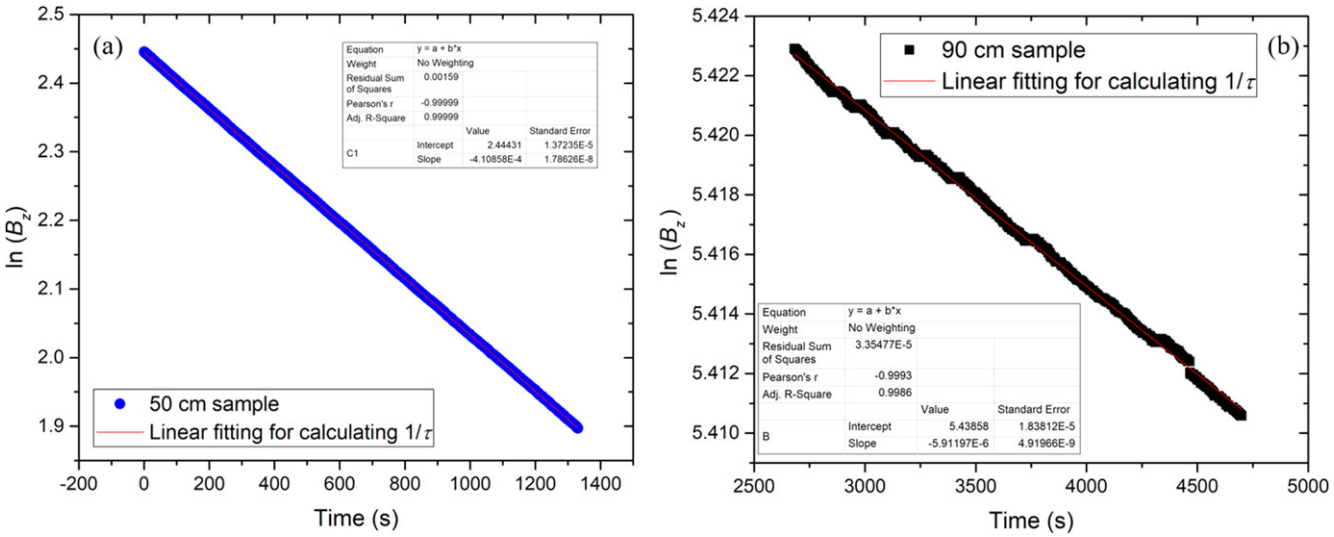

Figure 4. Typical field decay method results plotted in a $\ln(B) - t$ plot for closed-loop coils with joining length of (a) 50 cm, (b) 90 cm.

Table 2. Detailed simulation parameters for section 3.1.

Model category	Layer numbers	$\rho_e/\rho_{b1} \sim \rho_{b4}$ (Ω m)	$d_e/d_{b1} \sim d_{b4}$ (m)
Single layer model	a	1.5×10^{-9}	0.4×10^{-3}
Multilayer model	b1	0.4×10^{-9}	0.1×10^{-3}
	b2	0.8×10^{-9}	0.1×10^{-3}
	b3	1.6×10^{-9}	0.1×10^{-3}
	b4	3.2×10^{-9}	0.1×10^{-3}

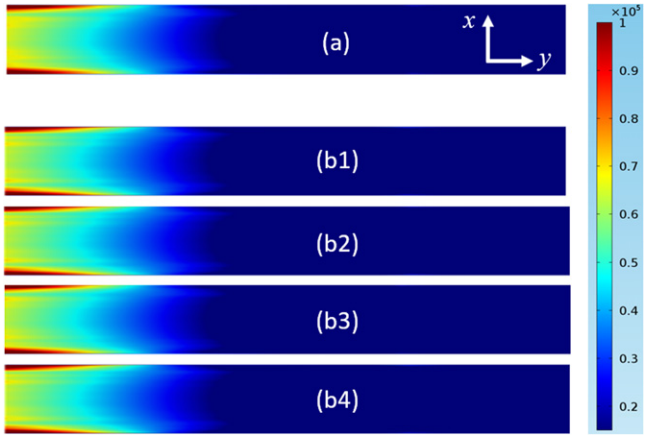

Figure 5. J_z distributions between the single layer model and multilayer model.

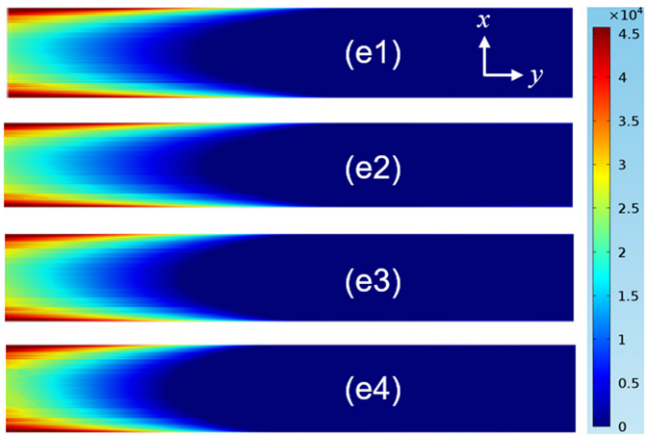

Figure 6. J_z distribution under different combinations of ρ_e and d_e (keeping ρ_s constant).

$\log(R_j)$–$\log(l)$ curves may be the same when ρ_e and d_e are varied but ρ_s is a constant value. Three kinds of $\log(R_j)$–$\log(l)$ curves based on the different ρ_s values (e: $\rho_s = 2.28 \times 10^{-12}\,\Omega\,m^2$, f:$\rho_s = 1.08 \times 10^{-10}\,\Omega\,m^2$, g: $\rho_s = 2.52 \times 10^{-11}\,\Omega\,m^2$) listed in table 3 are illustrated in figure 7. Because the values of ρ_s are relatively large, the $\log(R_j)$–$\log(l)$ curves of (f) and (g) are nearly linear, which is in accordance with equation (1). The $\log(R_j)$–$\log(l)$ curve of (e) shows a saturated phenomenon. Under the same values of ρ_s, the variation tendency and the lower limit of the (e1)–(e4) curves are nearly identical. The difference among the (e1)–(e4) curves is less than 0.1 nΩ, likely due to the meshing accuracy under different thickness cases in COMSOL. As a result, ρ_s is largely considered as the main determinant of the J_z distribution and the variation tendency of joint resistance along with overlap length.

Table 3. Detailed simulation parameters for section 3.2.

Analysis case	Subcases	ρ_s	Resistivity (Ω m)	Thickness (m)
e	e1	$2.28 \times 10^{-12}\ \Omega\ m^2$	1.2×10^{-8}	0.19×10^{-3}
	e2		6.6×10^{-9}	0.34×10^{-3}
	e3		2.5×10^{-9}	0.91×10^{-3}
	e4		9.8×10^{-10}	2.29×10^{-3}
g	—	$2.52 \times 10^{-11}\ \Omega\ m^2$	4.2×10^{-8}	0.6×10^{-3}
f	—	$1.08 \times 10^{-10}\ \Omega\ m^2$	1.8×10^{-7}	0.6×10^{-3}

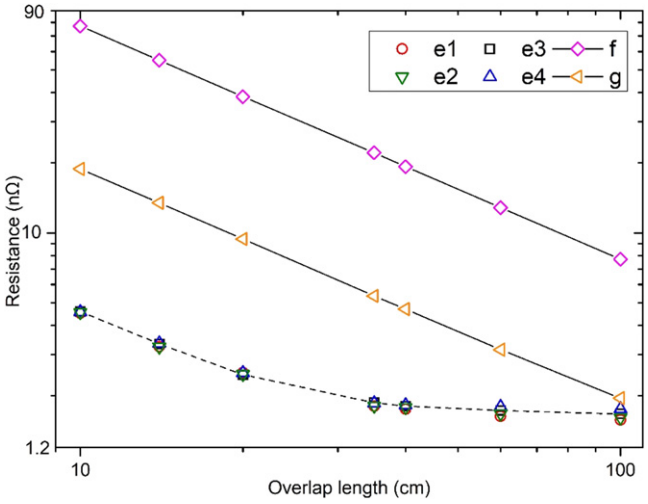

Figure 7. Relationship between joint resistance and overlap length under different ρ_e and d_e values (keeping ρ_s constant) in a log–log plot.

4. Experimental verification

The experimental results for joint samples with overlap lengths of 40–90 cm (the longer joints), which are determined by the field decay method, are listed in table 4 and marked by violet stars in figure 8. For joint samples with overlap lengths longer than 20 cm, in order to determine whether the $\log(R_j) - \log(l)$ curve is in agreement with equation (1) or the simulation results from our single-equivalent layer model, the value of R_j should be obtained if equation (1) holds.

Fifteen soldered lap joints with overlap lengths within 3–20 cm, for which equation (1) is expected to hold, are made and measured to calculate the value of ρ_s. The joint resistance values of these samples are also plotted in figure 8 and marked by black solid circles. These data exhibit a good linear relationship in the log–log plot. The value of R_j (longer than 40 cm) for the cases following equation (1) can be extrapolated. The uncertainty of the extrapolation value is important because it is necessary to distinguish the experimental results and calculated values from equation (1). The measurement uncertainty ΔR_j can be calculated by

$$\Delta R_j = t_\zeta s_{\overline{R_j}}, \tag{9}$$

where t_ζ is a factor corresponding with a 95% confidence level, and $s_{\overline{R_j}}$ is the standard error of the joint resistance, which is obtained from linear fitting. ΔR_j for joint samples within 3–20 cm are quite small ($\Delta R_j/R_j$ is small than 1%). It means that the linear fitting and the ρ_s calculated by linear fitting are reliable. The red dashed line in figure 8 illustrates this linearity, which follows equation (1). ρ_s can be calculated by its interception, and introduced in the single layer simulation model to predict the $\log(R_j)$–$\log(l)$ relationship, as shown by the blue line in figure 8. The detailed simulation parameters are listed in table 5. The most attractive characteristic is that the joint resistance tends to an asymptotic value of approximately 0.5–0.6 nΩ when the joining length is larger than 40 cm, in contrast to the behavior predicted by equation (1). It is also notable that the experimental resistance values of 40–90 cm joints obtained by the field decay method (violet stars in figure 8) meet the simulation values well.

For the longer joints extrapolated from shorter samples, the uncertainty Δy of R_j (l = 40, 50, 70, 90, and 100 cm in figure 8) ΔS_{Rj} is calculated by

$$\Delta s_{R_j} = \sqrt{(l^k \cdot \ln(10) \cdot 10^b \cdot \Delta s_k)^2 + (l^k \cdot \ln(l) \cdot 10^b \cdot \Delta s_b)^2}, \tag{10}$$

where k and b are the slope and intercept of linear fitting for the linear decreasing tendency. Δs_k and Δs_b are the standard error of the slope and intercept. In figure 8, black open circles with are the extrapolated joint resistance (40–100 cm) according to equation (1) and data corresponding to black solid circles. The ΔS_{Rj} are marked as error bars on black open circles. It is notable that the measurement values by the field decay method (l = 40–90 cm) are located beyond their confidence interval and significantly deviate from the red dashed line.

5. Discussion

5.1. The sensitivity of simulation results by different joint n values

The n values of the experimental soldered joints are different from the corresponding ones of the single YBCO tape because the joint's overall n value is also determined by the joint resistive parts. The typical n values of different joint lengths are listed in table 6 (using current data from 95% I_c to I_c). In order to determine the sensitivity of simulation results by different n values on the $\log(R_j)$–$\log(l)$ curves, we keep the other parameters (such as w and l) the same as those listed in table 7. Only the n values are changed in the simulation model; the R_j–l curves are plotted in figure 9. When n = 1,

Table 4. Detailed results for field decay method experiments (not including the shorter length joints).

	#1	#2	#3	#4	#5
l (cm)	40	50	60	75	90
Number of coil turns	14	9	7	70	83
L_{sim} (H)	1.92×10^{-5}	3.20×10^{-6}	7.20×10^{-6}	7.40×10^{-4}	1.90×10^{-4}
τ	1.37×10^{4}	2.42×10^{3}	6.21×10^{3}	6.67×10^{5}	1.67×10^{5}
R_j for bridge joint (nΩ)	1.4	1.32	1.16	1.12	1.14
R_j for lap joint (nΩ)	0.7	0.66	0.58	0.56	0.57

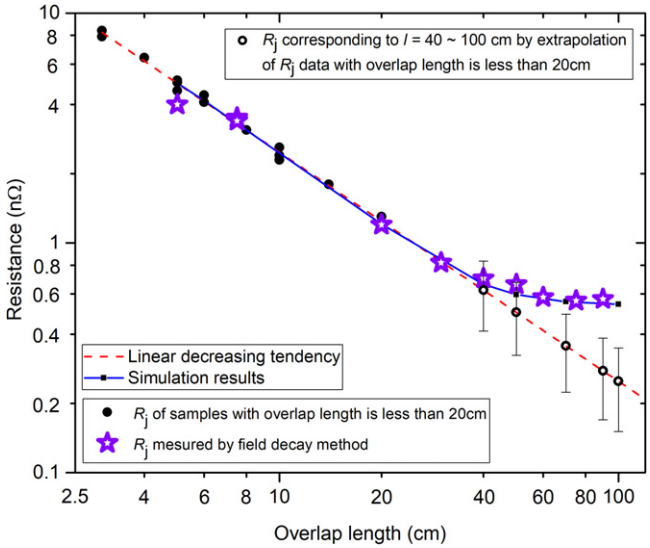

Figure 8. Comparison of experimental results and simulation results in a log–log plot. The ΔR_j is small and there is no need for plotting.

Table 5. Detailed parameters in simulation model for section 4.

Parameter	Value
ρ_s	2.47×10^{-12} Ω m^2
d_{YBCO}	0.01 mm
w	10 mm
I_j	100 A

Table 6. n values of various overlap length joints.

Overlap length	n value
0 cm (single YBCO tape)	39
1–10 cm	29–35
20 cm	23
40 cm	19
60 cm	14
100 cm	7

Table 7. Detailed parameters in simulation for section 5.2.

Parameter	Value
ρ_s	2.24×10^{-12} Ω m^2
d_{YBCO}	0.01 mm
w	10 mm
I_j	100 A

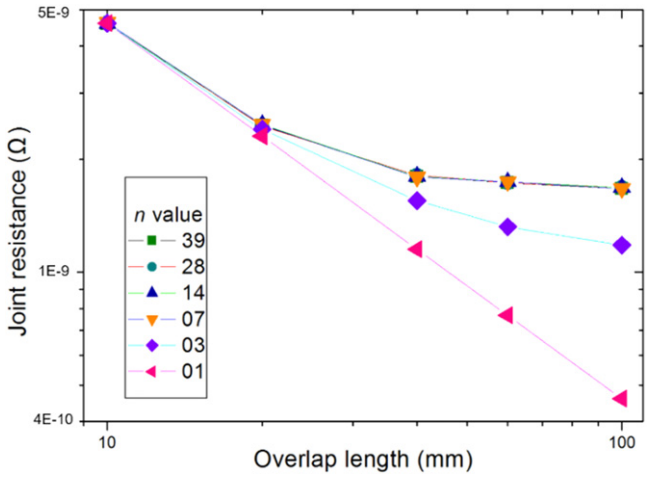

Figure 9. Log(R_j)–log(l) curve under different n values.

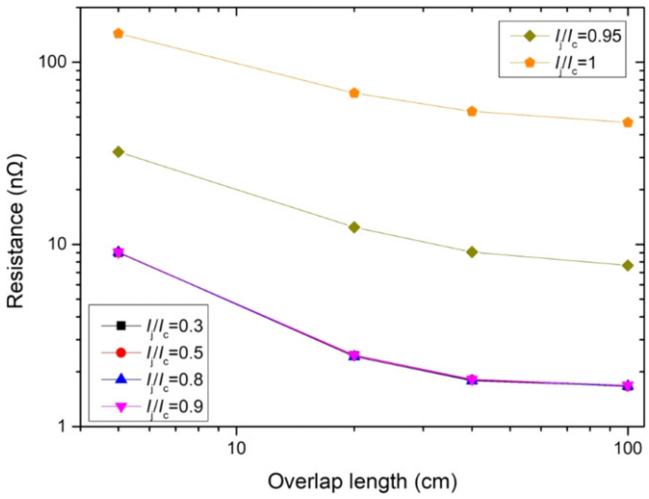

Figure 10. Log(R_j)–log(l) curves with different I_j/I_c values.

Table 8. Simulation results of a 50 mm joint with different I_j/I_c values.

I_j/I_c	R_j (nΩ)
0.3	9.02
0.5	9.05
0.8	9.06
0.9	9.09
0.95	32.23
1	143.7

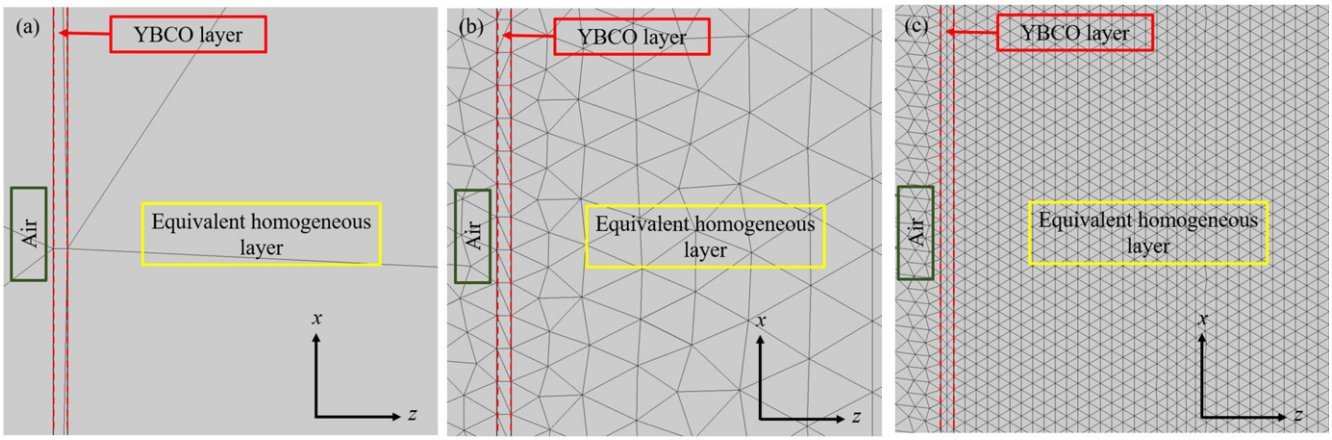

Figure 11. Meshing results of source faces with different element sizes: (a) model A, (b) model B, (c) model C.

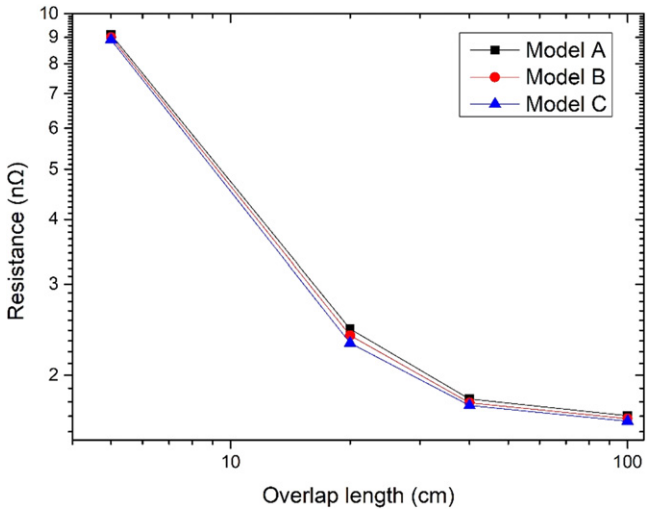

Figure 12. Simulation results of models A–C in a log–log plot.

Table 9. Detailed meshing parameters in simulation model A–C.

Model number	Max/min element size (mm)	DoF
A	7.7/0.56	1.4×10^5
B	0.05/0.01	1.8×10^6
C	0.01/0.001	9.8×10^6

Table 10. Meshed number and computing times between two models.

	Multilayer model	Single layer model
Meshed number	20 000	5000
Solved time	8 h	1 h

which can be considered as a non-superconducting material, its $\log(R_j)$–$\log(l)$ curve is linear, which corresponds with equation (1) (violet markers) in figure 9. As the n value increases, the $\log(R_j)$–$\log(l)$ curve tends to an asymptotic value. It is found that the simulation results exhibit a low sensitivity to the n value, provided that n is larger than 7. Therefore, we reasonably set $n = 39$ as a global parameter in all the joint models.

5.2. The sensitivity of simulation results by different values of I/I_c

The ratio between the input currents I_j and I_c should be taken into account because the YBCO effect is not negligible when $I_j \approx I_c$ [35]. Different values of I_j/I_c are set in a 5 cm joint model, and the other simulation parameters are the same as those in table 6. The joint resistance values are listed in table 8, and are almost identical when the value of I_j/I_c is less than 90%. Moreover, the $\log(R_j)$–$\log(l)$curves (which consist of $l = 5$, 20, 40, and 100 cm joints) are simulated with different I_j/I_c as shown in figure 10. The simulation results indicate that this model has a low sensitivity of I_j/I_c when I_j/I_c is less than 90%.

5.3. The sensitivity of simulation results by different meshing precision levels

Because the YBCO layers in a simulation model are relatively thin compared with the equivalent homogeneous layer, using the built-in element size in COMSOL such as 'finer' in the whole source face may lead to lower meshing quality for the YBCO layers as shown in figure 11(a). The YBCO layers are little divided in the z-axis. Although this kind of meshing method does not affect the convergence of subsequent simulation processes, the meshing precision still must be discussed.

Three kinds of element sizes are set in the simulation model; the detailed parameters and meshing graphics are shown in table 9 and figure 12. The simulation results shown in figure 12 (5, 20, 40, and 100 cm samples) are nearly identical, but the simulation time of model A is much smaller than those of model B and model C. In all cases, the $\log(R_j)$–$\log(l)$ curve exhibits a nonlinear relationship when the overlap length exceeds a certain threshold value, in contrast to the linear $\log(R_j)$– $\log(l)$ relationship when $R_j = \rho d/lw$ holds. Thus, it is sufficient to employ the built-in element size ('finer' level from COMSOL) in this study.

The single layer structure avoids the complex boundary conditions and reduces the computation remarkably. Moreover, this method solves convergence problems in COMSOL when meshing extremely thin sublayers. In the same mesh precision and other conditions, the computing times between these two models are listed in table 10.

6. Conclusion

This paper proposes an equivalent single homogenous layer model to simulate joint resistance for actual multilayer structure joints. According to equations (2)–(5), the line integral of bulk resistivity over the z-direction along the joint sublayers between YBCO layers can be described by a single resistance per unit of area ρ_s in one single-equivalent homogenized layer. The equivalence and validity of this simplified model is verified by: (1) the J_z distributions in different sublayers of the multilayer structure model are nearly coincident with the distribution obtained from the single layer model. (2) The parameters provided by short (5–20 cm) experimental soldered joints are used to simulate the joint resistance of the longer joints (20–100 cm). The simulation results match the experimental results well. Based on this model, our conclusions are: (1) when the overlap length of a resistive joint exceeds a certain threshold value, the joint resistance tends to an asymptotic value instead of a continued decrease; (2) the value of ρ_s is the main determinant of the J_z distribution and the variation tendency of $\log(R_j)$–$\log(l)$ curves.

Acknowledgments

This work was sponsored by the National Natural Science Foundation of China (51502171) and National Key Research and Development Program 2017YFB0902301.

ORCID iDs

Yunhao Pan https://orcid.org/0000-0002-3073-0771

References

[1] Brittles G D, Mousavi T, Grovenor C R M, Aksoy C and Speller S C 2015 Persistent current joints between technological superconductors *Supercond. Sci. Technol.* **28** 093001

[2] Senatore C, Alessandrini M, Lucarelli A, Tediosi R, Uglietti D and Iwasa Y 2014 Progresses and challenges in the development of high-field solenoidal magnets based on RE123 coated conductors *Supercond. Sci. Technol.* **27** 103001

[3] Kalsi S S, Gamble B B, Snitchler G and Ige S O 2006 The status of HTS ship propulsion motor developments *Proc. IEEE Power Eng. Soc. Gen. Meeting 2006*

[4] Iwasa Y, Bascnan J, Hahn S and Yao W 2009 High-temperature superconductors for NMR/MRI magnets: opportunities and challenges *Supercond. Cryog.* **11** 1–7

[5] Yanagisawa Y *et al* 2014 Operation of a 400 MHz NMR magnet using a (RE:rare earth) $Ba_2Cu_3O_{7-x}$ high-temperature superconducting coil: towards an ultra-compact super-high field NMR spectrometer operated beyond 1 GHz *J. Magn. Reson.* **249C** 38

[6] Liu J, Cheng J and Wang Q 2013 Evaluation of NbTi superconducting joints for 400 MHz NMR magnet *IEEE Trans. Appl. Supercond.* **23** 34–9

[7] Igarashi M, Nakao H, Terai M, Kuriyama T, Hanai S, Yamashita T and Yamagi M 2005 Persistent current HTS magnet cooled by cryocooler (1)—project overview *IEEE Trans. Appl. Supercond.* **15** 1469–72

[8] Kusada S *et al* 2005 Persistent current HTS magnet cooled by cryocooler (2)—magnet configuration and persistent current operation test *IEEE Trans. Appl. Supercond.* **15** 2285–8

[9] Tasaki K *et al* 2005 Persistent current HTS magnet cooled by cryocooler (3)—HTS magnet characteristics *IEEE Trans. Appl. Supercond.* **15** 2289–92

[10] Tosaka T, Tasaki K, Marukawa K, Kuriyama T, Nakao H, Yamaji M, Kurano K, Igarashi M, Nemoto K and Terai M 2005 Persistent current HTS magnet cooled by cryocooler (4)—persistent current switch characteristics *IEEE Trans. Appl. Supercond.* **15** 2293–6

[11] Jin X, Yanagisawa Y, Maeda H and Takano Y 2015 Development of a superconducting joint between a $GdBa_2Cu_3O_{7-\delta}$-coated conductor and $YBa_2Cu_3O_{7-\delta}$ bulk: towards a superconducting joint between RE (rare earth) $Ba_2Cu_3O_{7-\delta}$-coated conductors *Supercond. Sci. Technol.* **28** 075010

[12] Kim J H, Ji B K, Joo J, Yang C W and Nah W 2000 Superconducting joint between Bi–Pb–Sr–Ca–Cu–O superconductor tapes *IEEE Trans. Appl. Supercond.* **10** 1182–5

[13] Iida K, Yoshioka J, Sakai N and Murakami M 2002 Superconducting joint of Y–Ba–Cu–O superconductors using Er–Ba–Cu–O solder *Physica* C **370** 53–8

[14] Park Y, Lee M, Ann H, Choi Y H and Lee H 2014 A superconducting joint for $GdBa_2Cu_3O_{7-\delta}$-coated conductors *NPG Asia Mater.* **6** e98

[15] Zermeno V, Krüger P, Takayasu M and Grilli F 2014 Modeling and simulation of termination resistances in superconducting cables *Supercond. Sci. Technol.* **27** 124013

[16] Zheng J *et al* 2017 Low-resistance and strong-adhesion soldering of second-generation high-temperature superconductor tapes within a short time *IEEE Trans. Appl. Supercond.* **27** 6603706

[17] Tsui Y, Surrey E and Hampshire D 2016 Soldered joints—an essential component of demountable high temperature superconducting fusion magnets *Supercond. Sci. Technol.* **29** 075005

[18] Grilli F, Brambilla R, Sirois F, Stenvall A and Memiaghe S 2013 Development of a three-dimensional finite-element model for high-temperature superconductors based on the H -formulation *Cryogenics* **53** 142–7

[19] Zhang M and Coombs T A 2012 3D modeling of high-Tc superconductors by finite element software *Supercond. Sci. Technol.* **25** 015009

[20] Hong Z, Vanderbemden P, Pei R, Jiang Y, Campbell A M and Coombs T A 2008 The numerical modeling and measurement of demagnetization effect in bulk YBCO superconductors subjected to transverse field *IEEE Trans. Appl. Supercond.* **18** 1561–4

[21] Lu Y, Wang J, Wang S and Zheng J 2008 3D-modeling numerical solutions of electromagnetic behavior of HTSC bulk above permanent magnetic guideway *J. Supercond. Novel Magn.* **21** 467–72
[22] Wang Y, Song H, Yuan W, Jin Z and Hong Z 2017 Ramping turn-to-turn loss and magnetization loss of a no-insulation (RE) $Ba_2Cu_3O_x$ high temperature superconductor pancake coil *J. Appl. Phys.* **121** 113903
[23] Wang Y W, Zhang M, Yuan W J, Hong Z Y, Jin Z J and Song H H 2017 Non-uniform ramping losses and thermal optimization with turn-to-turn resistivity grading in a (RE) $Ba_2Cu_3O_x$ magnet consisting of multiple no-insulation pancake coils *J. Appl. Phys.* **122** 053902
[24] Miao Q, Zhu J M, Cheng M, Zhang Z, Li Z Y, Wang Y, Sheng J, Jin Z and Hong Z 2015 Fabrication and characteristic tests of a novel low-resistance joint structure for YBCO coated-conductors *IEEE Trans. Appl. Supercond.* **25** 6600705
[25] Pan Y, Sheng J, Wu W, Wang Y, Zeng W, Zhao Y, Zhang Z-W, Li Z, Hong Z and Jin Z 2017 Numerical study on simplified resistive joints of coated conductors: is there a lower limit of the joint resistance? *IEEE Trans. Appl. Supercond.* **27** 6601905
[26] Sheng J, Zeng W, Wu W, Ma J, Li Z, Jin Z and Hong Z 2016 Numerical study on silver diffusion joints of coated conductors by finite-element method *IEEE Trans. Appl. Supercond.* **26** 1–5
[27] Mei Z and Morris J W 1992 Characterization of eutectic Sn–Bi soldered joints *J. Electron. Mater.* **21** 599–607
[28] Lu J, Han K, Sheppard W R, Viouchkov Y L, Pickard K W and Markiewicz W D 2011 Lap joint resistance of YBCO coated conductors *IEEE Trans. Appl. Supercond.* **21** 3009–12
[29] Celentano G *et al* 2010 Electrical and mechanical characterization of coated conductors lap joints *IEEE Trans. Appl. Supercond.* **20** 1549–52
[30] Bagrets N, Augieri A, Celentano G, Tomassetti G, Weiss K P and della Corte A 2015 Investigation of ReBCO conductor tape joints for superconducting applications *IEEE Trans. Appl. Supercond.* **25** 6602705
[31] Michael P C, Qu T, Voccio J, Bascuñán J, Hahn S and Iwasa Y 2017 A REBCO persistent-current switch (PCS): test results and switch heater performance *IEEE Trans. Appl. Supercond.* **27** 0500705
[32] Qu T, Michael P C, Voccio J, Bascuñán J, Hahn S and Iwasa Y 2016 Persistent-current switch for pancake coils of rare earth-barium-copper-oxide high-temperature superconductor: design and test results of a double-pancake coil operated in liquid nitrogen (77–65 K) and in solid nitrogen (60–57 K) *Appl. Phys. Lett.* **109** 082601
[33] Kato J Y, Sakai N, Tajima S, Miyata S, Konishi M, Yamada Y, Chikumoto N, Nakao K, Izumi T and Shiohara Y 2006 Diffusion joint of YBCO coated conductors using stabilizing silver layers *Physica* C **445–448** 686–8
[34] Watanabe T, Kamata T, Maebatake T, Teranishi R, Kiss T, Yamada K, Kaneko K, Yoshizumi M and Izumi T 2013 Study of factors in joint resistance for GdBCO coated conductors *Phys. Proc.* **45** 165–8
[35] Kim Y B, Hempstead C F and Strnad A R 1965 Flux-flow resistance in type-II superconductors *Solid State Commun.* **65** 1171–3